Design of BET Inhibitor Prodrugs with Superior Efficacy and Devoid of Systemic Toxicities

Farrukh Vohidov,[1‡] Jannik N. Andersen,[2‡] Kyriakos D. Economides,[2] Michail V. Shipitsin,[2] Olga Burenkova,[2] James C. Ackley,[2] Bhavatarini Vangamudi,[2] Nolan M. Gallagher,[1] Peyton Shieh,[1] Matthew R. Golder,[1] Jenny Liu,[1,2] William K. Dahlberg,[2] Hung V.-T. Nguyen,[1] Deborah J. C. Ehrlich,[1] Julie Kim,[1] Sung Jin Huh,[2] Allison M. Neenan,[2] Joelle Baddour,[2] Sattanathan Paramasivan,[2] Elisa de Stanchina[3] Gaurab KC,[2] David J. Turnquist,[2] Jennifer K. Saucier-Sawyer,[2] Paul W. Kopesky,[2] Samantha W. Brady,[2] Michael J. Jessel[2], Lawrence A. Reiter,[2] Donald E. Chickering,[2] Jeremiah A. Johnson,[1*] Peter Blume-Jensen[2,4*]

[1]Department of Chemistry, Massachusetts Institute of Technology, 77 Massachusetts Avenue, Cambridge, Massachusetts 02139, United States

[2]XTuit Pharmaceuticals, 35 Gatehouse Drive, Waltham, Massachusetts 02451, United States

[3]Memorial Sloan Kettering Cancer Center, 417 E 68th St, New York, NY 10065, United States

[4]Current Address: Acrivon Therapeutics, Lab Central, 700 N. Main Street, Cambridge, MA 02139, United States

[‡]These authors contributed equally.

*Corresponding Authors: J.A. Johnson: jaj2109@mit.edu; P. Blume-Jensen: pblumejensen@acrivon.com

Abstract: Prodrugs engineered for preferential activation in diseased versus normal tissues offer immense potential to improve the therapeutic index of preclinical and clinical-stage active pharmaceutical ingredients that either cannot be developed otherwise or whose efficacy or tolerability it is highly desirable to improve. Such approaches, however, often suffer from trial-and-error design, precluding predictive design and optimization. Here, using BET bromodomain inhibitors (BETi)—a class of epigenetic regulators with proven anti-cancer activity but clinical development hindered by systemic adverse effects— we introduce a platform that overcomes these challenges. Through tuning of traceless linkers appended to a "brush prodrug" scaffold, we demonstrate that it is possible to correlate *in vitro* prodrug activation kinetics with *in vivo* tumor pharmacokinetics, leading to novel BETi prodrugs with enhanced anti-tumor efficacy and devoid of dose-limiting toxicities. This work has immediate clinical implications, introducing principles for the predictive design of prodrugs and potentially overcoming hurdles in drug development.

Significance: Prodrugs can be designed to modify essential biopharmaceutical properties and thus improve dependent absorption, distribution, metabolism, excretion, and toxicity (ADMET) of challenging-to-develop drug molecules. However, in conventional drug development programs, prodrug versions of lead compounds are often explored as a last option, after significant amounts

of resources and precious time have already been unsuccessfully invested. We demonstrate that prodrugs can be designed to improve the therapeutic efficacy and tolerability of drug molecules held back in the clinical development by their narrow therapeutic windows. Importantly, we demonstrate that, if used early in development, prodrugs can enable rapid access to proof of concept *in vivo* experiments, thus promising accelerated translational timelines and more efficient use of resources.

Main Text: An essential part of drug discovery is medicinal chemistry optimization to deliver a drug candidate for clinical testing and ultimate regulatory approval (1-3). This process, which often fails, is typically costly and time consuming and follows trial-and-error optimization, leading to a trade-off between orthogonally-trending properties such as target potency, solubility, metabolic stability, and toxicity (4, 5). For example, BETis have been the subject of intense medicinal chemistry efforts, displaying broad preclinical efficacy (6) *in vivo*, as well as clinical activity in various cancers, including notably myelofibrosis (7, 8). BETi treatment has been shown to cause drug-dependent decreases in the expression of oncogenes such as c-MYC (9-11) and cyclin-dependent kinases (12-14). To date, at least 23 structurally distinct BETi have been evaluated in >46 human clinical trials demonstrating clinical efficacy of this class of drugs, despite severe dose-limiting toxicities. A review of www.clinicaltrials.gov from January 2017 to May 2020 indicates that most of these programs report protracted phase I/II development times and reduced patient enrollment targets due to severe dose-limiting toxicities (DLTs) (Supplementary Table 1). For example, the prototypical benzodiazepine BETi OTX-015 (MK-8628, Merck) (15-17) causes thrombocytopenia (96%), anemia (91%), and neutropenia (51%), with additional gastro-intestinal adverse events (diarrhea, vomiting and mucositis) (18). Similar treatment-related adverse effects have been reported for the bivalent BETi, AZD5153 (19, 20). Given the promising clinical activity of this drug class, we envisioned that a rational prodrug approach to improve the TI of existing clinical and preclinical BETi could be an immediately actionable strategy to enable their successful clinical development.

The development of covalent drug-delivery systems, or prodrugs, often also involves trial-and-error design due to unpredictable active pharmaceutical ingredient (API) carrier interactions, limited synthetic scalability and modularity, and unpredictable or poorly controlled prodrug activation profiles (21, 22). Here, we introduce a modular, scalable, stoichiometrically-defined bottle brush prodrug (BPD) platform that overcome these challenges. Through the synthesis of BETi-BPDs carrying either OTX-015 or a bivalent BETi "T-API" conjugated through molecularly optimized, traceless linkers, we exemplify an accelerated method to improve the TI of BETi as demonstrated using orthotopically implanted, immune-competent tumor-bearing mice. This work establishes BPDs as a promising, widely applicable solution for small molecule API delivery to overcome DLTs and improve the safety profile for compounds with proven

clinical activity (as demonstrated for OTX-015) and for the accelerated development of novel lead candidates (as demonstrated using T-API).

Results. Downregulation of the c-Myc oncogene and subsequent cell cycle arrest has been proposed as a major mechanism for BETi-mediated tumor growth inhibition (9, 23, 24); however, downregulation of c-Myc in normal tissues, including gut and hematopoietic precursors in bone marrow result in clinically observed on-target DLTs (8, 11). We hypothesized that improved delivery of BETi-BPDs to tumors combined with the design of linkers with favorable API release in cancer compared to normal tissues would be key parameters to improve the TI. To test this hypothesis, OTX-015 offered an attractive starting point for BETi-BPD development, given the inferior TI of this compound that has hindered its successful clinical development.

Optimization of API release rates through rational traceless linker editing. OTX-015 contains a phenolic substituent suitable for direct conjugation to our polyethylene glycol (PEG)-*branch*-alkyne macromonomers (MMs) that constitute the basic building blocks of the BPD platform (Fig. 1a). Four different azido acids were used to prepare four OTX-015-conjugated macromonomers (MMs) with *in vitro* half-lives of OTX-015 release ($t_{1/2,MM}$) of 5 h (MM **B1**) to 6 d (MM **B4**) in phosphate-buffered saline at 37 °C (Fig. 1b,c). BETi-BPDs **B1**–**B4** were prepared through ring-opening metathesis polymerization (ROMP) (25-28) of each MM at a target degree of polymerization (DP) of 10. Trace amounts (1 mol %) of Cy7.5 fluorophore-labeled MM (29) were included in all ROMP reactions to enable downstream *in vivo* tissue imaging studies to supplement our quantitative pharmacokinetics (PK) analyses for accurate biodistribution (BD) assessment. Near complete conversions of MM to BETi-BPD were observed for each MM (Fig. S1). The ROMP reaction parameters were adjusted so that the hydrodynamic diameter (D_h) of **B4** was tuned in at 13 nm as determined by dynamic light scattering (DLS) (Fig. S2). This size range is comparable to therapeutic antibodies and ADCs, offering a clinically proven BD, PK, and disease tissue penetration. In support of the scalability of this approach, 4 g of BETi-BPDs were readily prepared for subsequent biological studies (Fig. S3). As expected for BPDs were the APIs are shielded by hydrophilic PEG, the half-maximal inhibitory concentrations (IC_{50}) for **B1**–**B4** were approximately one order-of-magnitude higher compared to the parent API based on *in vitro* viability assays using either bone marrow $CD34^+$ progenitor cells (erythroid, megakaryocyte, and myeloid), human aortic endothelial cells, lymphoma (SU-DHL-2) or breast cancer (4T1) cells (Fig. S4,5)

To assess the pharmacological properties of BETi-BPDs *in vivo*, we dosed BALB/c mice orthotopically implanted with syngenic 4T1 tumors with **B2**–**B4** and collected blood samples at multiple time points for PK analysis by mass spectrometry (MS). As shown in Fig. 1d, **B4** was relatively stable with minimal free peak drug blood concentration detected systemically 30 min after administration, which is significantly

lower than the peak concentrations at 2 and 3 h post dosing of maximally tolerated doses (MTD) of OTX-015. In contrast, **B2** and **B3** displayed 2–3 times higher concentrations of free OTX-015 in serum. **B1** was not evaluated *in vivo* due to its rapid API release in buffer (Fig. 1c). In parallel to the blood analyses, the tumor tissue concentrations of free OTX-015 were quantified 72 h post dose (Fig. 1e). The tumor API levels released from **B4** at 72 h were comparable with the tumor drug concentrations at 2 to 3 h after oral administration (Fig. 1e). Thus, **B4** exhibits a long-term, depot-like release of therapeutically relevant drug concentrations at least up to 72 h.

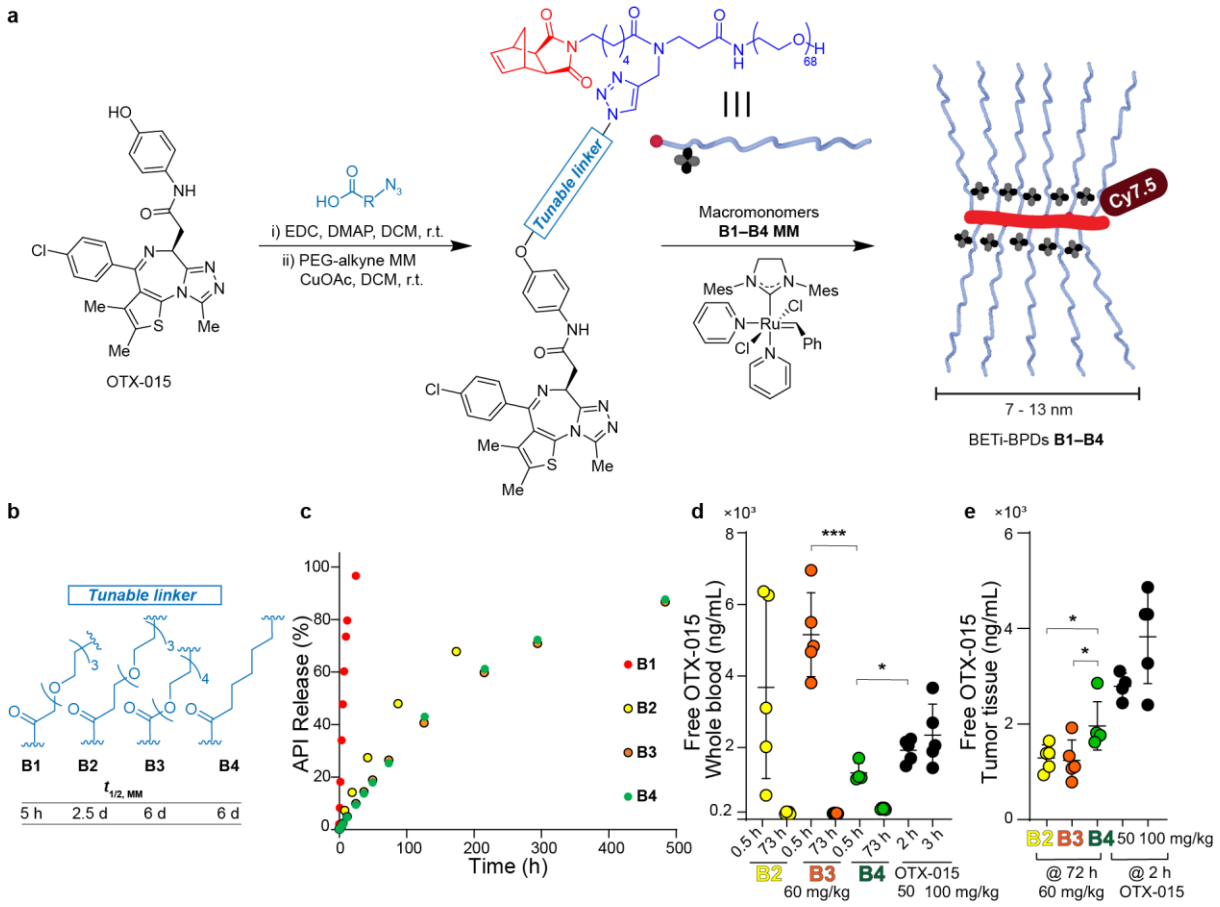

Figure 1. **Design, synthesis, and OTX-015 release profiles for BETi-BPDs B1–B4. a,** Design and synthesis of OTX-015-based brush prodrugs **B1–B4**. Azido-acids (shown in blue) are used to form ester or carbonate conjugates with OTX-015. Cu-catalyzed azide-alkyne cycloaddition to a PEG-alkyne macromonomer (MM) generates **B1–B4 MM**s. Ring-opening metathesis polymerization (ROMP) of each MM in the presence of a Cy7.5-labeled MM (1 mol %) generates BETi-BPDs **B1–B4**. **b,** Careful linker design enables rational modulation of OTX-015 release half-lives. **c,** Release of BET inhibitors *in vitro* (saline buffer, 37 °C). **d,** Linker chemistry modulates serum stability. Blood levels of free OTX-015 drug released from **B4** at peak concentration (0.5 h post administration) is lower than the peak concentrations observed after equivalent doses of **B2**, **B3**, and lower compared to the maximum tolerated p.o. dose of OTX-015 at 2 or 3 h. **e, B4** displays higher levels of released OTX-015 in tumor tissue compared to **B2** and **B3**, 72 hours after last dose of brush prodrugs. Statistical analysis performed using unpaired *t* test. Any p-values not shown are n.s.; * p<0.05, *** p<0.001; error bars represent SD.

To further confirm that the different tumor concentrations of released API from the similar-sized **B2**, **B3**, and **B4** are primarily due to their linker design rather than differences in the overall biodistribution, *ex vivo* near-infrared fluorescence imaging of tissue samples was conducted to determine the amount of Cy7.5 fluorophore-labeled prodrug present. All three BETi-BPDs (**B2**, **B3**, and **B4)** showed similar accumulation in tumor tissue based on whole tumor analysis (Fig. S6). Importantly, fluorescence imaging of intact tumors and organs and of homogenized tissues showed preferential distribution of BETi-BPDs to orthotopic tumors and only negligible levels of Cy7.5 in bone marrow and the gut—organs associated with the DLTs of OTX-015 (Fig. 2a,b). These results, combined with the *in vitro* release kinetics for **B4**, demonstrate that it is possible to chemically fine-tune both the BD of, and API release from, BETi-BPDs to minimize systemic exposure while maintaining, or even improving, tumor exposure of the active drug.

Superior anti-tumor efficacy of B4 *in vivo*. We next evaluated the anti-tumor efficacy of **B4** in the aggressive 4T1 syngeneic, orthotopic model, which recapitulates many features of late stage triple-negative breast cancer (TNBC) in humans. These mice have a functioning adaptive immune system and therefore also provide an opportunity to study potential treatment-related immunosuppressive adverse effects. A dose escalation study using **B4** was conducted in randomized, tumor-bearing BALB/c mice dosed with equivalents of OTX-015 at 15, 30, or 60 mg/kg twice per week for two weeks for a total of 4 doses, or at 60 mg/kg three times per week for two weeks for a total of 6 doses (Fig. 2c). Two separate control cohorts were dosed for 14 days with free OTX-015 twice a day by oral gavage (bid; po) at 100 or 200 mg/kg, respectively, mimicking the clinical route of administration.

A dose-proportional anti-tumor efficacy was observed for mice administered **B4**, with highly effective tumor growth inhibition at higher doses (Fig. 2d). At the 60 mg/kg OTX-015 equivalent dose of **B4,** both the 4× and 6× regimens showed superior anti-tumor efficacy compared with the highest daily tolerated dose of OTX-015 (100 mg/kg bid). Notably, the total amount of OTX-015 in the group that received the highest dose of **B4** was ~360 mg/kg, which is *>7-fold less than* that of the group given OTX-015 at 100 mg/kg bid (2800 mg/kg after two weeks) (Fig. 2d). We attribute the enhanced efficacy with less dosage-equivalent of API to the linker-optimized depot effect, wherein **B4** accumulates in tumor tissue and releases therapeutically relevant concentrations of OTX-015 over longer time periods than what is achievable with OTX-015, even when dosed twice daily. To support this concept, MS analyses of homogenized tumor samples (Fig. 2e) revealed high levels (~100 µg/g) of **B4** (BETi-BPD) and ~3 orders-of-magnitude lower levels of released API (free OTX-015 ~1500 ng/g). Moreover, the amount of **B4** and released API in tumor samples scaled proportionally with dosage (Fig. 2e). Notably, the concentration of free OTX-015 72 h after **B4** injection is still almost 50% of the peak concentration in tumors achieved from non-tolerated orally dosed OTX-015 obtained at 2 h post dosing and much greater than the concentration of oral OTX-015 at MTD, which is cleared from the tumor tissue and cannot be detected after 24 h (Fig. 2e). As a direct

consequence of the optimal BD and API release from **B4** in tumor versus other tissues, no weight loss was observed in any of the groups receiving **B4**, while the group receiving free OTX-015 at 200 mg/kg had to be sacrificed early due to severe weight loss (>20%); the group receiving the highest tolerated dose of API at 100 mg/kg experienced diarrhea and modest (~5%) weight loss after 2 weeks of chronic dosing (Fig. 2f).

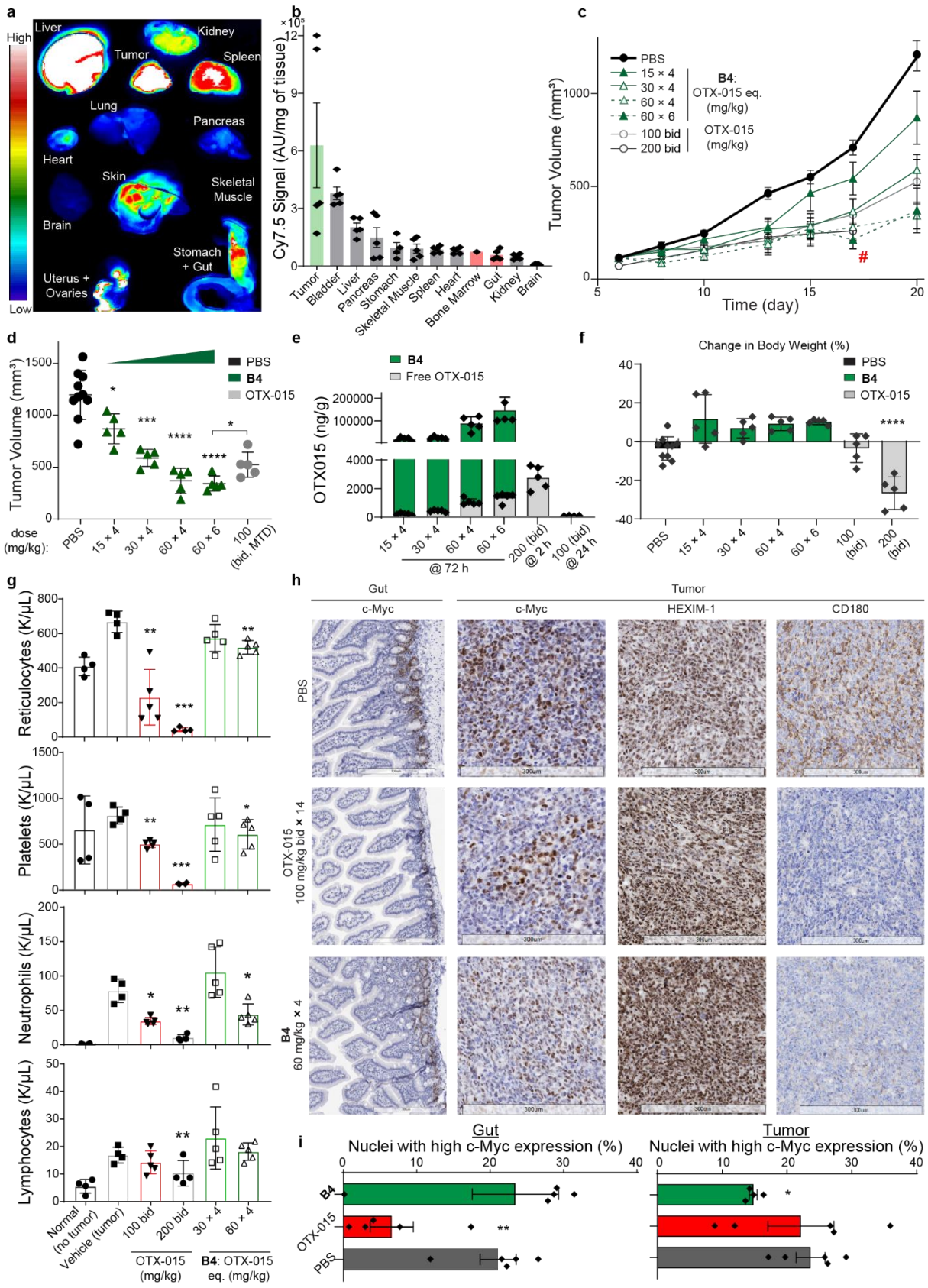

Figure 2. Tissue imaging and PK/PD/Efficacy studies of BETi-BPDs releasing OTX-015. a, Representative whole organ fluorescent imaging of Cy7.5-labled **B4** in tumor and indicated organs (Cy7.5 IVIS; $\lambda_{ex/em}$ = 745/800 nm). **b,** Biodistribution of **B4** quantified

using fluorescence signal (n=5) in homogenized tissue samples normalized by tissue weight; gut and bone marrow labeled in red font to highlight their low biodistribution; error bars represent SE. **c,d,** Anti-tumor efficacy in 4T1 orthotopic breast carcinoma model (Balb/C mice). **B4** was dosed i.v. with equivalents of OTX-015 at 15 mg/kg, 30 mg/kg, or 60 mg/kg, twice per week for two weeks for a total of 4 doses, or at 60 mg/kg every other day for two weeks for a total of 6 doses to mice (n=5 pr group) randomized with pre-treatment tumor sizes of 100 mm^3 (BPDs contain ~12% wt. of OTX-015; 500 mg/kg dose BPD is 60 mg/kg API equivalent). OTX-015 was dosed twice daily by oral gavage (bid; po). **e,** Tumor PK of **B4** prodrug. BETi-BPD provides sustained release of API at the tumor site, and the levels of free OTX-015 at 72 h after injection are close to 50% of the peak concentration of the parent drug OTX-015 2 h are an oral dosage of 200 mg/kg bid. **f,** No weight loss was observed in any of the **B4** regimens, while the maximum tolerated dose of API (100 mg/kg) caused diarrhea and some weight loss. #: The OTX-015 200-mg/kg bid cohort was taken down after eleven days due severe weight loss. **g,** Analysis of blood cell populations demonstrates that unlike the parent free OTX-015 drug, the **B4** prodrug does not cause the systemic toxicity associated with BET inhibition. No reduction in platelet, reticulocyte, neutrophil, and lymphocyte levels were detected (n=5) at doses resulting in superior anti-tumor efficacy of **B4** compared to free API; error bars represent SD. **h,i, B4** causes only minimal intestinal toxicity compared to OTX-015 as evidenced by in situ protein expression of c-Myc, a PD biomarker for BET inhibition, in the base of crypts and preserved colonic villus epithelial surface morphology. Anti-tumor efficacy of **B4** prodrug is comparable to free OTX-015 as shown by modulation of PD markers c-Myc, HEXIM1, and CD180 levels in extracted tumors. Statistical analysis performed using unpaired *t* test for tumor volumes and c-Myc expression and using Welch's *t* test for assessment of hematologic toxicity; all groups compared to the vehicle group except where indicated otherwise. Any p-values not shown are n.s.; * p<0.05, ** p<0.01, *** p<0.001, **** p<0.001. Scale bars: 300 μm.

BETi-BPDs releasing OTX-015 exhibit enhanced anti-tumor efficacy without dose-limiting bone marrow and intestinal toxicities. Detailed analyses of cell populations in terminal blood and bone marrow collected from the above efficacy study demonstrated that animals dosed with **B4** were spared from the systemic DLTs normally associated with clinical BET inhibition (Fig. 2g, Fig. S7). Specifically, platelet, reticulocyte, neutrophil, and lymphocyte levels were not affected in mice treated with **B4** compared to the group treated with OTX-015. Moreover, tissue samples from gut and tumors were collected for immunohistochemical analyses (Fig. 2h,i). **B4** induced minimal intestinal toxicity compared to OTX-015, as evidenced by preserved colonic villus epithelial cell surface morphology and *in situ* expression of c-Myc in the base of crypts. Consistent with the anti-tumor efficacy of **B4**, a robust modulation of known pharmacodynamic (PD) markers was observed in tumor tissue, with downregulation of c-Myc and CD180 and upregulation of HEXIM1 (30) (Fig. 2i, Fig. S8). In conclusion, **B4** represents a promising BETi prodrug with an expanded TI and improved efficacy following infrequent dosing.

The BPD platform applied to preclinical (triazolopyridizine-based) bivalent BETi. We next turned our attention to testing the ability of our platform to expedite the optimization of a different BETi. AstraZeneca reported a triazolopyridazine (20) class of potent BETi that are structurally distinct from OTX-015, comprising bivalent ligands that engage both of the bromodomains (31) of the BET family of proteins and displaying higher potencies in cell-based assays compared to many of the other small-molecule inhibitors derived from the benzodiazepine scaffold. AZD5153, a bivalent BETi with optimized PK properties, is currently undergoing clinical trials (19). For our study, we selected an AZD5153 derivative "T-API" (Fig. 3a), which features a trifluoromethyl substituent in place of a methoxy group. While T-API has similar *in vitro* potency compared to AZD5153 (Fig. S5, S9) (IC_{50} < 100 nM) against the multiple myeloma (MM1.S) cell line, it suffers from poor physicochemical properties such as low aqueous solubility (<0.05 mg/mL),

high lipophilicity (log $D_{7.4}$ > 4.2), and inadequate hepatocyte stability (70 heps Cl_{int} mL/min/10^6 cells) (20), all of which are largely prohibitive for activity *in vivo* (Fig. S10). We found that blood levels of T-API in BALB/c mice (n = 3) were significantly lower compared to AZD5153 (1000 ng/mL vs. 5000 ng/mL) 2 h after 10 mg/kg i.v. administration and the exposure dropped to negligible levels within 4 h (Fig. S11a), most likely due to rapid metabolism in liver (20) (Fig. S12). Having already demonstrated that our BPD platform provides for both favorable delivery of BETi-BPDs and subsequent API release in tumor tissues, we next evaluated whether we could improve the efficacy of T-API with low metabolic stability and rapid clearance.

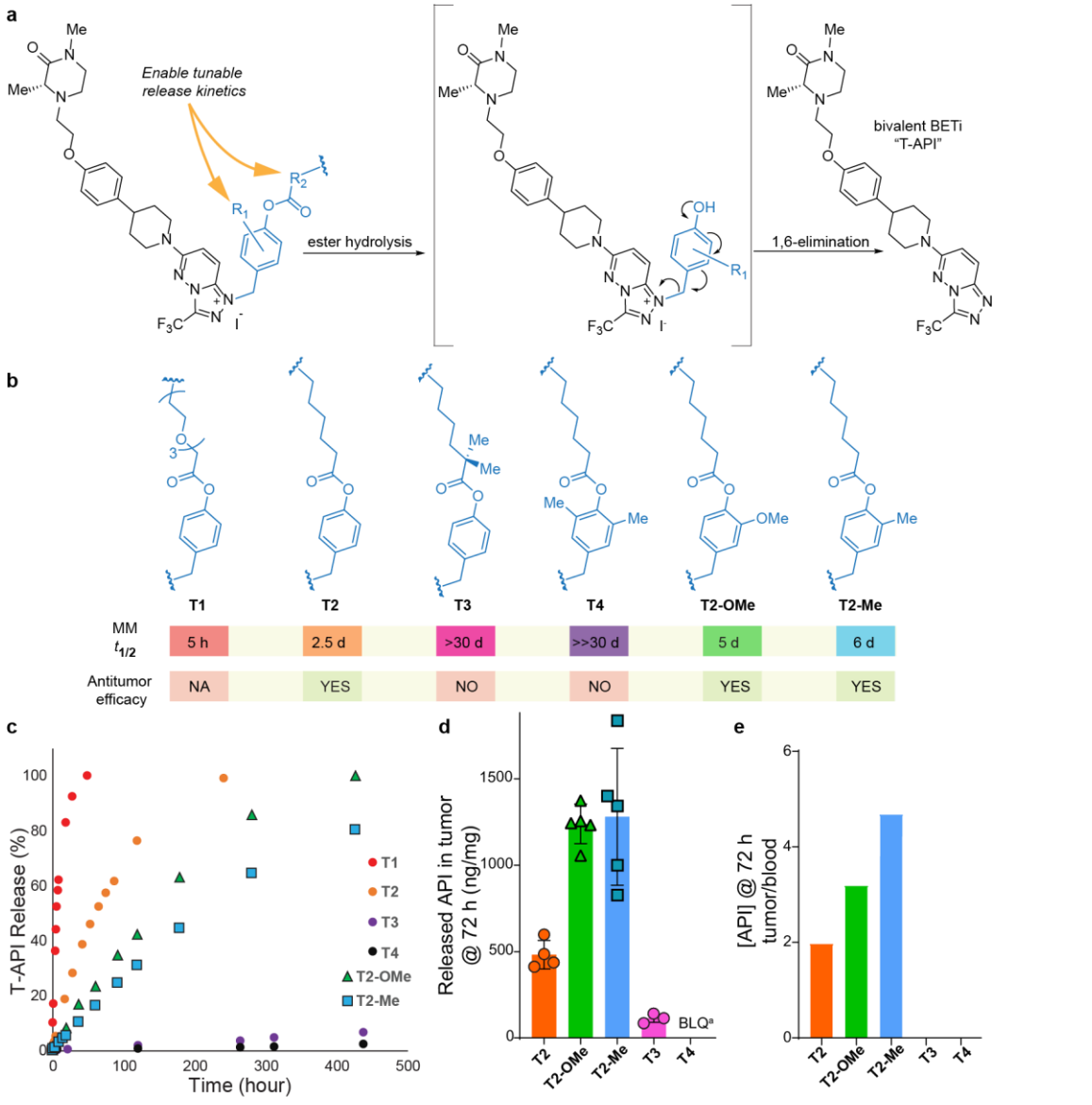

Figure 3. Phenyl ester traceless linker editing for optimized T-API release. a, Drug release mechanism via 1,6-elimination from triazolopyridazinium salts conjugates in **T**-series brush prodrugs. **b,** Modulation of release kinetics of the T-API via linker chemistry. **c,** Release of T-API inhibitor *in vitro* (saline buffer, 37 °C). **d,** Released T-API in tumors 72 h after the last dose in 60 mg/kg × 4 treatment groups (n=5). Concentration of released T-API at the tumor site is finely tuned via linker chemistry; error

bars represent SD. **e,** Ratios of released T-API in the tumor relative to whole blood. Brush prodrugs offer favorable accumulation and differential release in the tumor. [a]: below limit of quantification.

Unlike OTX-015, T-API (Fig. 3a; black structure) does not offer an obvious synthetic handle for BPD conjugation. To address this challenge, and inspired by recent amide-based linkers for N-containing drugs (32, 33), we developed a new class of phenyl ester linkers based on the quaternization of nitrogen-containing heterocycles using benzyl iodides (Fig. 3a; blue structure). For these linkers, prodrug activation is dependent on the rate-determining cleavage of a *para*-aryl ester, which can be tuned through rational modifications to the ester, followed by a 1,6-elimination cascade (34), releasing the drug via *N*-debenzylation (Fig. 3a). The desired T-API-based triazolopyridazinium salts were synthesized in 50–70% isolated yields following optimized benzylation procedures (see Supplementary Materials for details; Fig. S13, S14). Their structures were unambiguously determined by 2D NMR spectroscopy (Materials and Methods); regardless of linker used, quaternization was observed to occur on the same nitrogen atom of the 1,2,4-triazole of T-API (Fig. 3a). The T-API conjugates were converted to MMs and later to their corresponding BETi-BPDs via ROMP (Fig. S1); the D_h of **T2** was 7 nm as determined by DLS (Fig. S2).

Using this novel conjugation chemistry and rational design of linker steric and electronic properties, we initially prepared four different T-API-conjugated MMs with $t_{1/2,MM}$ tuned from hours (**T1**) to days (**T2**) to months (**T3** and **T4**) (Fig. 3b) as confirmed by *in vitro* drug release assays (saline buffer, 37 °C) (Fig. 3c). For each linker, free T-API was observed to be the sole species released upon hydrolysis (Fig. S15), suggesting 1,6-elimination occurs rapidly under physiologically relevant conditions. Following i.v. administration (60 mg/kg × 4 of T-API equivalent) to mice bearing 4T1 tumors, **T3** and **T4** showed negligible to low levels of free T-API in tumor tissues (Fig. 3d), presumably due to the slow hydrolysis of their linkers. In contrast, **T2** released therapeutically relevant concentrations of T-API in tumor tissue resulting in an attractive tumor-to-blood ratio of 2:1 (Fig. 3e), suggesting this to be the preferred linker of this series (note: **T1** was not studied *in vivo* due to its very rapid release kinetics). Notably, for the *in vivo* studies, the clinical candidate AZD5153 was selected as the benchmark for T-API prodrug since the poor ADMET properties of T-API is not compatible with in vivo efficacy studies (Fig. S11, S12). Consistent with the clinical dosing schedule (daily or twice daily) for AZD5153 (19), this API was not detectable 24 h after administration (Fig. S11b). By contrast, the PK profile in blood following a single dose of **T2** (15 mg/kg T-API equivalent, i.v.) demonstrated that this BETi-BPD released only very low levels of T-API in blood with a peak concentration significantly lower than that of the rapidly cleared AZD5153 (Fig. S11b).

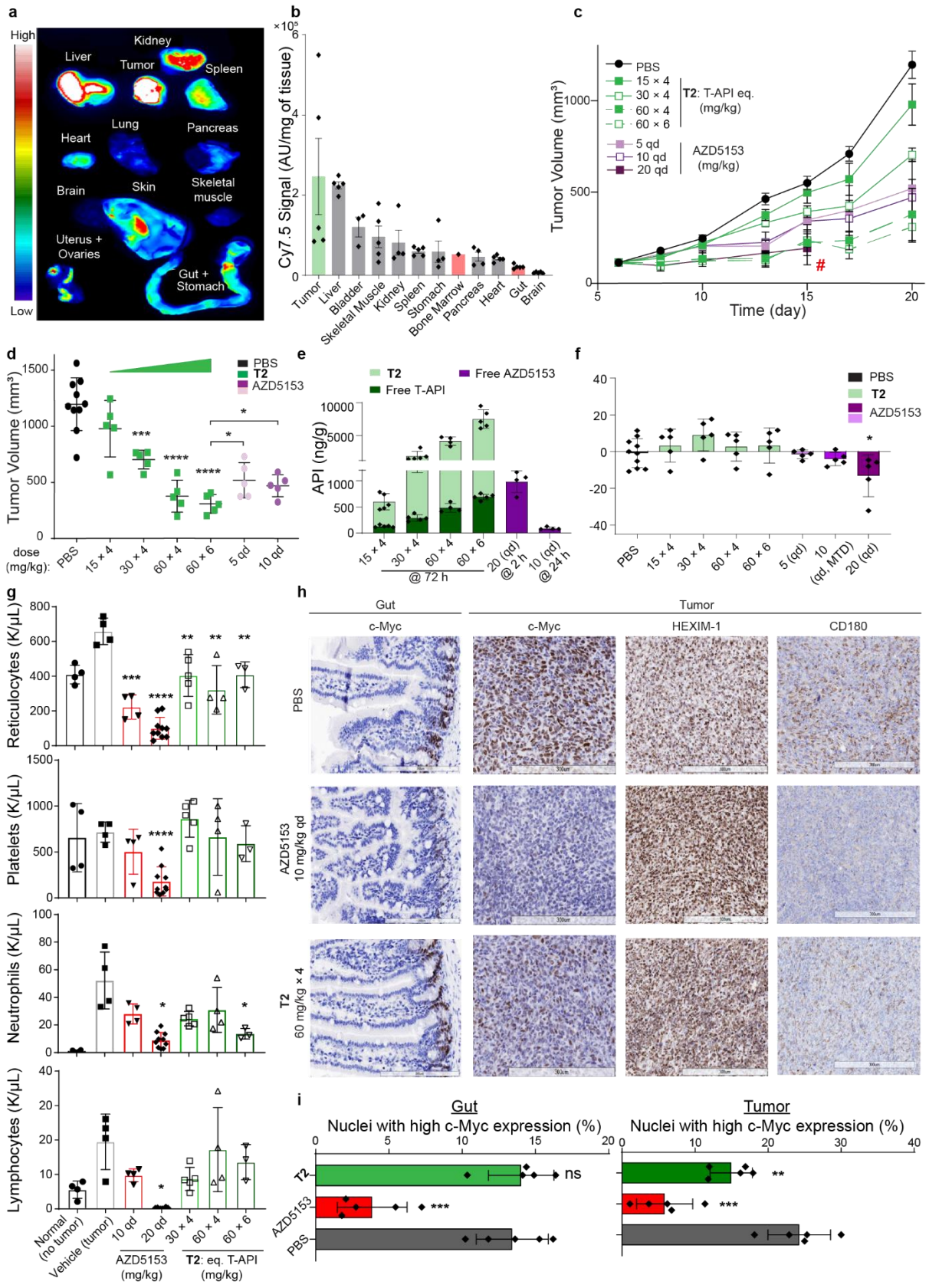

Figure 4. **Tissue imaging and PK/PD/Efficacy studies of BETi-BPDs releasing the AZD5153-derivative T-API. a,** Representative whole organ Cy7.5 fluorescent imaging showing favorable accumulation of the **T2** prodrug in tumor. **b,** Biodistribution of the **T2**

quantified using fluorescence signal (n=5) in homogenized tissue samples normalized by tissue weight; gut and bone marrow labeled in red font to highlight their low biodistribution; error bars represent SE. **c,d,** Efficacy in 4T1 orthotopic breast carcinoma model in Balb/C mice. **T2** was dosed with T-API equivalents at 15 mg/kg, 30 mg/kg, or 60 mg/kg, twice per week for two weeks for a total of 4 doses, or at 60 mg/kg every other day for two weeks for a total of 6 doses to mice randomized with tumor sizes of 100 mm^3 (BPDs contain ~12% wt. of T-API; 500 mg/kg dose BPD is 60 mg/kg API equivalent). AZD5153 was dosed qd as a PO bolus. **e,** Tumor pharmacokinetics of **T2** Brush prodrug. Brush provides sustained release of T-API at the tumor site, and the levels of free active drug at 72h after injection are comparable to the peak concentration of tumor AZD5153 (at 2 h post dosing) at the non-tolerated dosage of 20 mg/kg qd. **f,** No significant weight loss was observed in any of the **T2** regimens, while the highest tolerated dose of API at 10 mg/kg caused diarrhea and showed some weight loss. #: AZD5153 20-mg/kg cohort was taken down after ten days due severe weight loss. **g,** Analysis of blood cell populations demonstrates that, unlike free AZD5153, **T2** Brush prodrug does not cause systemic toxicity normally associated with BET inhibition in bone marrow. No reduction in platelet, reticulocyte, neutrophil, and lymphocyte levels were detected (n=5) at doses resulting in superior anti-tumor efficacy of **T2** compared to free AZD5153; error bars represent SD. **h,i, T2** causes only minimal intestinal toxicity compared to OTX-015 as evidenced by *in situ* protein expression of c-Myc, biomarker for BET inhibition, in the base of crypts and preserved colonic villus epithelial surface morphology. Anti-tumor efficacy of **T2** prodrug is comparable to free AZD5153 as shown by modulation of PD markers c-Myc, HEXIM1, and CD180 levels in extracted tumors. Statistical analysis performed using unpaired *t* test for tumor volumes and c-Myc expression and using Welch's *t* test for assessment of hematologic toxicity; all groups compared to the vehicle group except where indicated otherwise. Any p-values not shown are n.s.; * $p<0.05$, ** $p<0.01$, *** $p<0.001$, **** $p<0.0001$. Scale bars: 300 μm.

Similar to the OTX-015 derived BETi-BPD **B4**, **T2** displayed favorable tumor accumulation based on Cy7.5 imaging (Fig. 4a,b). Additionally, **T2** (dosed i.v. with equivalent of T-API at 60 mg/kg × 6, 360 mg/kg cumulative dose) showed better anti-tumor efficacy compared with maximum tolerated daily dose (qd) of AZD5153 (10 mg/kg, p.o. 130 mg/kg cumulative dose; Fig. 4c and 4d), which is notable given that the latter compound underwent extensive medicinal chemistry optimization. To further validate the critical nature of the **T2** linker, prodrugs **T3** and **T4** (60 mg/kg × 4) were also tested in the same tumor model. These constructs displayed no antitumor efficacy (Fig. S16), consistent with MS analysis of extracted tumors showing minimal release of free T-API despite similar levels of **T3** and **T4** prodrugs in tumor compared to **T2** (Fig. S17). In contrast, **T2** generated therapeutically relevant and superior concentrations of T-API that remained at high concentrations (~10× more) in tumor tissue 72 h following administration. Again, negligible levels of AZD5153 were detectable in tumor tissue after 24 h (Fig. 4e). Importantly, mice administered the high dose of **T2** (60 mg/kg × 6) displayed no weight loss (Fig. 4f). While AZD5153 also achieved objective tumor responses when dosed at 5–20 mg/kg (po, qd; 65–360 mg/kg cumulative doses), these animals experienced significant body weight loss and the group receiving 20 mg/kg had to be taken down before the end of the study. In contrast to the MTD dose group (10 mg/kg po qd of AZD5153), which led to significant reductions in white blood cell, platelet, and reticulocyte counts, dosing with **T2** displayed no discernible blood toxicity (Fig. 4g). Moreover, detailed analysis of gut and tumor samples demonstrated that **T2** lowers c-Myc levels in tumors but not in the gut, while AZD5153 displayed PD biomarker modulation in both tumor and gut epithelial tissue (Fig. 4h,i). Overall, these results for **T2** mirror those of **B4** yet with a structurally different BETi, validating the drug agnostic nature of our platform and showing its potential for accelerating the development of APIs with poor ADMET without protracted medicinal chemistry optimization.

Closer analysis of the tumor PK data for **B4** and **T2** (Fig. 2e and 4e, respectively) revealed much less **T2** and free T-API 72 h after administration compared to **B4** and free OTX-015, suggesting that the rate of linker cleavage for **T2** may be unnecessarily high despite its excellent *in vivo* efficacy. Seeking to further improve this system, we rationally designed and synthesized two new variants of **T2** with electron donating *ortho*-methoxy (**T2-OMe**) and *ortho*-methyl (**T2-Me**) substituents (Fig. 3b) that are expected to slow the rate of ester hydrolysis. Accordingly, *in vitro* release assays revealed a doubling of the $t_{1/2,MM}$ values to ~5 and ~6 days for **T2-OMe** and **T2-Me**, respectively (Fig. 3c), confirming that such rational design can be used to fine tune T-API release in this system. Moreover, tumor and blood PK studies showed further improved T-API release (Fig. 3d) and higher tumor:blood ratios (up to ~5 compared to ~2 for **T2**, Fig. 3e) for these constructs compared to **T2**. In agreement with these improved tumor PK results, lower doses of **T2-OMe** (60 mg/kg x 4) and **T2-Me** (60 mg/kg x 4) compared to **T2** (60 mg/kg x 6) led to improved or similar tumor growth inhibition (Fig. 5a,b), respectively and no gross toxicity (Fig. 5c) compared to high daily dose (10 mg/kg qd, 130 mg/kg cumulative dose) of AZD5153.

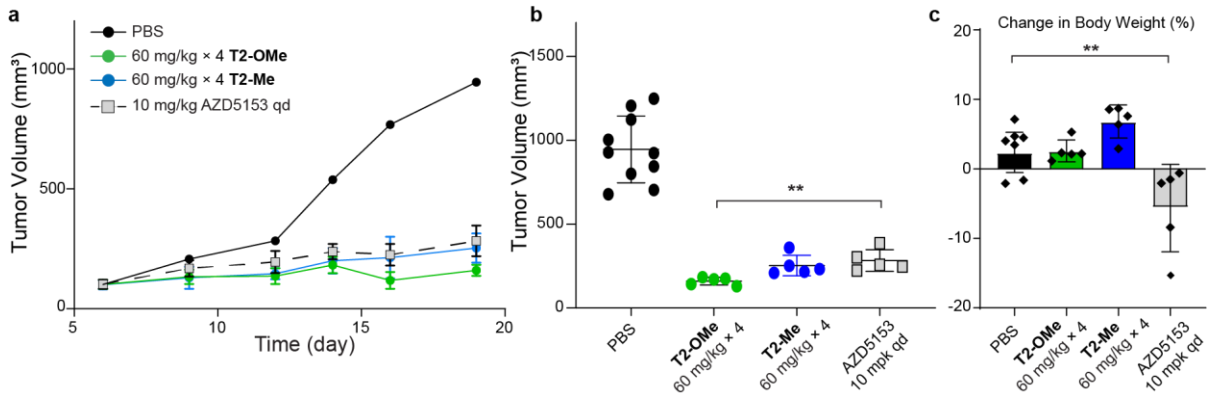

Figure 5. a,b, Brush prodrugs **T2-OMe** and **T2-Me** display improved tumor growth inhibition after fewer doses compared to AZD5153. BPDs were dosed at 60 mg/kg equivalent of T-API twice per week for two weeks for a total of 4 doses to Balb/C mice bearing 4T1 orthotopic tumors; AZD5153 was dosed at 10 mg/kg qd as a PO bolus. **c,** No significant weight loss was observed in any of the **T2-Ome** and **T2-Me** regimens, while the highest tolerated dose of API at 10 mg/kg caused diarrhea and showed some weight loss. Error bars represent SD. Statistical analysis performed using unpaired *t* test; * p<0.05, ** p<0.01.

CONCLUSION

Prodrugs with improved biodistribution and preferential release of API in the diseased tissue offer great potential across all stages of drug development (35, 36). In principle, advanced assets with demonstrated clinical activity but whose development has been hindered by too narrow TI should be possible to successfully develop as optimized prodrugs (37). In the case of drug classes, like BETi, that have been tested in a vast number of clinical trials the health-economic and drug development cost implications are immense. Moreover, optimized prodrug versions of APIs can be generated preclinically to overcome ADMET challenges and provide a rapid route to proof-of-concept *in vivo* testing and potentially an accelerated translation to the clinic of drugs with significantly improved properties through such rational design.

In this work, we introduce a versatile and modular prodrug platform widely applicable to APIs and demonstrate the ability to significantly enhance the TI of both a clinical asset and a preclinical compound. Specifically, we overcome the narrow TI of BET inhibitors by rationally designing a series of macromolecular prodrugs based on a novel bottlebrush polymer platform. BET inhibitors have shown great potential as anti-cancer agents with durable tumor responses observed in some patients. Despite great interest from pharmaceutical companies, no BET inhibitor has advanced to late-stage trials due to reported high-grade side effects in patients. A notable exception to this trend is the BETi CPI-0610, which is being advanced in the clinic for myelofibrosis, hence leveraging the otherwise non-desirable activity in the bone marrow (NCT02158858). Similarly, many other promising drug candidates are often hindered from entering clinical practice by undesired toxicity to healthy cells, with 24% of drugs failing in clinical trials due to an inadequate clinical safety (38). Here, we were able to conjugate and deliver two structurally different BET inhibitors, optimizing linker chemistries for enhanced antitumor efficacies and improved TI.

Furthermore, we demonstrate that by molecular tuning of traceless linkers it is possible to achieve differential release of an API with limited release in blood and normal tissues, and yet favorable, sustained release at efficacious concentrations in the disease tissues. This approach stands in contrast to the use of targeting ligands to achieve tissue-selective therapy; through careful linker design, combined with size control of our BPDs for optimal biodistribution (see further below), improved TIs can be achieved even without tissue-targeting ligand engineering. Currently, we use optimized ester linkers that exhibit significant cleavage in tumor tissue, consistent with studies reporting generally increased activity of esterases, in particular carboxylesterases of the serine hydrolase superfamily, in tumors (39). We further developed a novel conjugation protocol with phenyl ester benzyl iodides via quaternary ammonium salt formation. We anticipate that our optimized procedure with good yields and high purity for synthesis of such prodrug conjugates with desirable properties will be widely applicable beyond the BETi drug class, while merger with additional targeting strategies may even further improve upon these systems in the future.

We are also able to fine-tune the size of our BETi-BPD prodrugs and have found preferential accumulation with ~10 nm hydrodynamic diameters, a size regime that is comparable to ADCs, in tumor tissue, achieving a drug depot-like accumulation in tumor tissues while at the same time minimizing drug exposure to nascent cell populations in bone marrow and gut, further improving their therapeutic window. Importantly, this work establishes practicality of decoupling of the physicochemical properties of an API from its biological activity. For example, we demonstrate how inherent poor physicochemical properties and rapid clearance of T-API can be turned into an advantage, minimizing the toxicity of the drug molecules escaping into systemic circulation. A related strategy for managing cytopenia was evaluated using INCB054329 (40). a small molecule BET inhibitor reported to have a short half-life, but without a means to selectively target the drug into tumors, interpatient variability prevented identification of an effective dosing regimen and the

trial was terminated. Collectively, our data suggest that the properties of BETi-BPDs warrant further investigation to enable translation into the clinic and that our BPD platform is widely applicable across APIs to generate prodrugs with significantly improved TI.

References and Notes:

1. C. A. Lipinski, F. Lombardo, B. W. Dominy, P. J. Feeney, Experimental and computational approaches to estimate solubility and permeability in drug discovery and development settings. *Adv. Drug Delivery Rev.* **23**, 3-25 (1997).
2. W. P. Walters, Going further than Lipinski's rule in drug design. *Expert Opinion on Drug Discovery* **7**, 99-107 (2012).
3. J. Hodgson, ADMET—turning chemicals into drugs. *Nat. Biotechnol.* **19**, 722-726 (2001).
4. M. M. Hann, G. M. Keserü, Finding the sweet spot: the role of nature and nurture in medicinal chemistry. *Nat. Rev. Drug Discovery* **11**, 355-365 (2012).
5. J. F. Pritchard *et al.*, Making Better Drugs: Decision Gates in Non-Clinical Drug Development. *Nat. Rev. Drug Discovery* **2**, 542-553 (2003).
6. A. Alqahtani *et al.*, Bromodomain and extra-terminal motif inhibitors: a review of preclinical and clinical advances in cancer therapy. *Future Sci. OA* **5**, FSO372 (2019).
7. M. Kleppe *et al.*, Dual Targeting of Oncogenic Activation and Inflammatory Signaling Increases Therapeutic Efficacy in Myeloproliferative Neoplasms. *Cancer Cell* **33**, 29-43.e27 (2018).
8. A. G. Cochran, A. R. Conery, R. J. Sims, Bromodomains: a new target class for drug development. *Nat. Rev. Drug Discovery* 10.1038/s41573-019-0030-7 (2019).
9. Jake E. Delmore *et al.*, BET Bromodomain Inhibition as a Therapeutic Strategy to Target c-Myc. *Cell* **146**, 904-917 (2011).
10. P. Filippakopoulos *et al.*, Selective inhibition of BET bromodomains. *Nature* **468**, 1067-1073 (2010).
11. Y. Xu, C. R. Vakoc, Targeting Cancer Cells with BET Bromodomain Inhibitors. *Cold Spring Harb. Perspect. Med.* **7** (2017).
12. A. Stathis, F. Bertoni, BET Proteins as Targets for Anticancer Treatment. *Cancer Discov.* **8**, 24-36 (2018).
13. W. Fiskus *et al.*, BET Protein Antagonist JQ1 Is Synergistically Lethal with FLT3 Tyrosine Kinase Inhibitor (TKI) and Overcomes Resistance to FLT3-TKI in AML Cells Expressing FLT-ITD. *Mol. Cancer Ther.* **13**, 2315-2327 (2014).
14. F. Kato *et al.*, MYCL is a target of a BET bromodomain inhibitor, JQ1, on growth suppression efficacy in small cell lung cancer cells. *Oncotarget* **7** (2016).
15. J. K. Noel *et al.*, Abstract C244: Development of the BET bromodomain inhibitor OTX015. *Mol. Cancer Ther.* **12**, C244-C244 (2013).
16. C. Berthon *et al.*, Bromodomain inhibitor OTX015 in patients with acute leukaemia: a dose-escalation, phase 1 study. *Lancet Haematol.* **3**, e186-e195 (2016).
17. J. Lewin *et al.*, Phase Ib Trial With Birabresib, a Small-Molecule Inhibitor of Bromodomain and Extraterminal Proteins, in Patients With Selected Advanced Solid Tumors. *J. Clin. Oncol.* **36**, 3007-3014 (2018).
18. S. Amorim *et al.*, Bromodomain inhibitor OTX015 in patients with lymphoma or multiple myeloma: a dose-escalation, open-label, pharmacokinetic, phase 1 study. *Lancet Haematol.* **3**, e196-e204 (2016).
19. J. S.-Z. Wang *et al.*, First-in-human study of AZD5153, a small molecule inhibitor of bromodomain protein 4 (BRD4), in patients (pts) with relapsed/refractory (RR) malignant solid tumor and lymphoma: Preliminary data. *J. Clin. Oncol.* **37**, 3085-3085 (2019).

20. R. H. Bradbury *et al.*, Optimization of a Series of Bivalent Triazolopyridazine Based Bromodomain and Extraterminal Inhibitors: The Discovery of (3R)-4-[2-[4-[1-(3-Methoxy-[1,2,4]triazolo[4,3-b]pyridazin-6-yl)-4-piperidyl]phenoxy]ethyl]-1,3-dimethyl-piperazin-2-one (AZD5153). *J. Med. Chem.* **59**, 7801-7817 (2016).
21. J. Shi, P. W. Kantoff, R. Wooster, O. C. Farokhzad, Cancer nanomedicine: progress, challenges and opportunities. *Nat. Rev. Cancer* **17**, 20 (2016).
22. S. Tran, P.-J. DeGiovanni, B. Piel, P. Rai, Cancer nanomedicine: a review of recent success in drug delivery. *Clin. Transl. Med.* **6**, 44 (2017).
23. D. S. Tyler *et al.*, Click chemistry enables preclinical evaluation of targeted epigenetic therapies. *Science* **356**, 1397-1401 (2017).
24. J. Shi, Christopher R. Vakoc, The Mechanisms behind the Therapeutic Activity of BET Bromodomain Inhibition. *Mol. Cell* **54**, 728-736 (2014).
25. J. A. Love, J. P. Morgan, T. M. Trnka, R. H. Grubbs, A Practical and Highly Active Ruthenium-Based Catalyst that Effects the Cross Metathesis of Acrylonitrile. *Angew. Chem., Int. Ed.* **41**, 4035-4037 (2002).
26. K. Kawamoto, M. Zhong, R. Wang, B. D. Olsen, J. A. Johnson, Loops versus Branch Functionality in Model Click Hydrogels. *Macromolecules* **48**, 8980-8988 (2015).
27. J. A. Johnson *et al.*, Drug-Loaded, Bivalent-Bottle-Brush Polymers by Graft-through ROMP. *Macromolecules* **43**, 10326-10335 (2010).
28. H. V. T. Nguyen *et al.*, Scalable Synthesis of Multivalent Macromonomers for ROMP. *ACS Macro Lett.* **7**, 472-476 (2018).
29. F. Vohidov *et al.*, ABC triblock bottlebrush copolymer-based injectable hydrogels: design, synthesis, and application to expanding the therapeutic index of cancer immunochemotherapy. *Chemical Science* **11**, 5974-5986 (2020).
30. T. C. Yeh *et al.*, Identification of CCR2 and CD180 as Robust Pharmacodynamic Tumor and Blood Biomarkers for Clinical Use with BRD4/BET Inhibitors. *Clin. Cancer. Res.* **23**, 1025-1035 (2017).
31. M. J. Waring *et al.*, Potent and selective bivalent inhibitors of BET bromodomains. *Nat. Chem. Biol.* **12**, 1097 (2016).
32. L. R. Staben *et al.*, Targeted drug delivery through the traceless release of tertiary and heteroaryl amines from antibody–drug conjugates. *Nature Chem.* **8**, 1112 (2016).
33. P. J. Burke *et al.*, Development of Novel Quaternary Ammonium Linkers for Antibody–Drug Conjugates. *Mol. Cancer Ther.* **15**, 938-945 (2016).
34. R. B. Greenwald *et al.*, Drug Delivery Systems Employing 1,4- or 1,6-Elimination: Poly(ethylene glycol) Prodrugs of Amine-Containing Compounds. *J. Med. Chem.* **42**, 3657-3667 (1999).
35. I. Ekladious, Y. L. Colson, M. W. Grinstaff, Polymer-drug conjugate therapeutics: advances, insights and prospects. *Nat. Rev. Drug Discov.* **18**, 273-294 (2019).
36. R. Duncan, Polymer conjugates as anticancer nanomedicines. *Nat. Rev. Cancer* **6**, 688-701 (2006).
37. J. Rautio, N. A. Meanwell, L. Di, M. J. Hageman, The expanding role of prodrugs in contemporary drug design and development. *Nat. Rev. Drug Discovery* **17**, 559-587 (2018).
38. R. K. Harrison, Phase II and phase III failures: 2013–2015. *Nat. Rev. Drug Discovery* **15**, 817 (2016).
39. D. Wang *et al.*, Human carboxylesterases: a comprehensive review. *Acta Pharmaceutica Sinica B* **8**, 699-712 (2018).
40. P. C. Liu *et al.*, Abstract 3523: Discovery of a novel BET inhibitor INCB054329. *Cancer Res.* **75**, 3523-3523 (2015).

Acknowledgements: We thank Dr. Bruce Adams for assistance with NMR analysis, and Drs. Robert Langer, Rakesh Jain, and Ronald Evans for critical review and support of this work.

Funding: We thank XTuit Pharmaceuticals for support of this work. J.A.J. thanks the National Institutes of Health (1R01CA220468-01) for support.

Author contributions: J.N.A. and P.B-J. conceived of the idea to develop BETi prodrugs. J.A.J. conceived of the bottlebrush prodrug platform used in this work. F.V. and J.A.J. designed the synthetic methods for BETi conjugation. J.N.A., F.V., J.A.J., and P.B.-J. developed the overall study design. F.V., N.M.G., P.S., M.R.G., H.V.T.N., D.J.C.E., and J.K. synthesized prodrugs. F.V., N.M.G., P.S, J.L., J.K.S.S., P.W.K., L.A.R., and D.E.C. characterized prodrugs. J.N.A, P.B.-J., PK.D.E., M.V.S., O.B., J.C.A., B.V., W.K.D., S.J.H., A.M.N., J.D., E.S., G.K., D.J.T., S.W.B., M.J.J., designed and performed in vitro and in vivo experiments. S.P performed LC-MS analysis of homogenized tissues and blood samples. F.V., J.N.A., J.A.J., and P.B-J. wrote the manuscript. All authors read and revised the manuscript.

Competing interests: F.V. and J.A.J. are named inventors on patent applications filed by the Massachusetts Institute of Technology on the linker compositions and bottlebrush polymer platform described in this work.

Data and materials availability: All data supporting the findings of this study are available within the Article, Supplementary Materials, Materials and Methods, and/or from the corresponding author upon reasonable request. Supplementary Materials contains data directly referenced in the Article (Fig S1-S17), while Materials and Methods contains synthetic methods and experimental procedures as well as detailed characterizations of the bottlebrush prodrugs.

Author Information

Correspondence and requests for materials should be addressed to J.A.J (jaj2109@mit.edu) and P.B.-J. (pblumejensen@acrivon.com).